





Cite this: *Nanoscale*, 2023, 15, 8395

# Spontaneous valley polarization and valley-nonequilibrium quantum anomalous Hall effect in Janus monolayer ScBrI $\ddagger$

Kang Jia, <sup>a</sup> Xiao-Jing Dong, <sup>a</sup> Sheng-Shi Li, <sup>b</sup> Wei-Xiao Ji <sup>b</sup> and Chang-Wen Zhang<sup>\*a,b</sup>

Topology and ferrovalley (FV) are two essential concepts in emerging device applications and the fundamental research field. To date, relevant reports are extremely rare about the coupling of FV and topology in a single system. By Monte Carlo (MC) simulations and first-principles calculations, a stable intrinsic FV ScBrI semiconductor with high Curie temperature ( $T_C$ ) is predicted. Because of the combination of spin-orbital coupling (SOC) and exchange interaction, the Janus monolayer ScBrI shows a spontaneous valley polarization of 90 meV, which is located in the top valence band. For the magnetization direction perpendicular to the plane, the changes from FV to half-valley-metal (HVM), to valley-nonequilibrium quantum anomalous Hall effect (VQAHE), to HVM, and to FV can be induced by strain engineering. It is worth noting that there are no particular valley polarization and VQAHE states for in-plane (IP) magnetic anisotropy. By obtaining the real magnetic anisotropy energy (MAE) under different strains, due to spontaneous valley polarization, intrinsic out-of-plane (OOP) magnetic anisotropy, a chiral edge state, and a unit Chern number, the VQAHE can reliably appear between two HVM states. The increasing strains can induce VQAHE, which can be clarified by a band inversion between  $d_{x^2-y^2}/d_{xy}$  and  $d_{z^2}$  orbitals, and a sign-reversible Berry curvature. Once synthesized, the Janus monolayer ScBrI would find more significant applications in topological electronic, valleytronic, and spintronic nanodevices.

Received 25th December 2022,

Accepted 10th April 2023

DOI: 10.1039/d2nr07221a

rsc.li/nanoscale

## 1. Introduction

Two-dimensional (2D) materials have raised a surge of research studies, partially for the great technological expectations for the integration and miniaturization of multiple functional nanodevices because of the successful separation of graphene.<sup>1–3</sup> In order to better process information, manipulating and exploiting the valley degree of freedom for low-energy carriers have gained special interest.<sup>4–6</sup> Among numerous 2D materials,<sup>7–13</sup> 2H-phase transition metal dichalcogenides (TMDs)  $\text{MX}_2$ , not only reveal great application prospects but also offer an intriguing platform to investigate novel physical phenomena due to their tunable and exceptional properties.<sup>14–17</sup> Because of inversion asymmetry, the valley degrees of freedom originating from the degenerate energy extrema for the corners of the hexagonal Brillouin zone (BZ)

present in those systems as strong spin-orbital coupling (SOC). For the sake of utilizing the valley index, it is crucial to remove the energy degeneracy in inequivalent valleys by means of breaking time reversal symmetry. Some attempts have been adopted *via* extrinsically inducing valley polarization in paravalley materials, such as optical pumping as well as magnetic doping, static magnetic field, and magnetic proximity effect.<sup>18–23</sup> However, these extrinsic means are very fragile and not easy to control precisely in experiments, hindering practical application in nonvolatile spintronic and valleytronic devices of low energy consumption and high storage density.

The discovery of 2D intrinsic ferromagnetic (FM) transition-metal layered materials has opened the door to address the above difficulties, for example,  $\text{Cr}_2\text{Ge}_2\text{Te}_6$ <sup>24</sup> and  $\text{CrI}_3$ .<sup>25</sup> In addition, robust FM order was recently found in the 2H-VSe<sub>2</sub> system, which can persist above room temperature.<sup>26</sup> For a typical hexagonal material of inversion symmetry breaking, the violation of time-reversal symmetry can be produced by spin-valley coupling, giving the ferrovalley (FV) semiconductor 2H-VSe<sub>2</sub> spontaneous valley polarization in wide applications towards the integration of valleytronics and spintronics.<sup>27</sup> Nevertheless, as emerging members in the 2D ferroic family, the room-temperature FV semiconductors are only discovered in a minority of hexagonal materials, such as  $\text{VSi}_2\text{N}_4$ ,<sup>28</sup>

<sup>a</sup>School of Physics and Physical Engineering, Qufu Normal University, Qufu, Shandong, 273100, People's Republic of China

<sup>b</sup>School of Physics and Technology, Institute of Spintronics, University of Jinan, Jinan, Shandong, 250022, People's Republic of China.

E-mail: ss\_zhangchw@ujn.edu.cn

$\ddagger$  Electronic supplementary information (ESI) available. See DOI: <https://doi.org/10.1039/d2nr07221a>

2H-CeI<sub>2</sub>,<sup>29</sup> 2H-LaBrI,<sup>30</sup> and 2H-FeClBr,<sup>31</sup> *etc.* Most of these reported materials possess FM-ordered in-plane (IP) magnetization, which is not conducive to realize spontaneous valley polarization, or the valley polarization is too small to overcome the thermal noise at room temperature. Consequently, it is imminently desirable to discover alternative intrinsic 2D FV candidates with sizable valley polarization, out-of-plane (OOP) FM ordering, and high Curie temperature ( $T_C$ ) simultaneously.

In consideration of the fundamental significance of topology in materials science and condensed matter physics, it is very interesting to combine topology and FV in some material systems, which is likely to generate emerging applications and novel physics.<sup>32</sup> Recently, some theoretical studies have been initiated to forecast topological phase transitions together with diverse magneto-valley coupling (MVC) states by utilizing external means, such as strain engineering, light modulation, and electronic correlation effects, as observed in 2H-ScI<sub>2</sub>,<sup>33</sup> 2H-FeCl<sub>2</sub>,<sup>34,35</sup> 2H-FeClF,<sup>36</sup> VSi<sub>2</sub>(N, P)<sub>4</sub>,<sup>37-39</sup> 2H-RuClBr,<sup>40</sup> and 2H-RuBr<sub>2</sub>.<sup>41</sup> Consequently, it is very necessary to further seek those topological nontrivial FV materials to explore the valley-dependent transport properties and quantum phase transitions for both practical nanodevice applications and fundamental scientific interest.

We appreciate that the Janus monolayer ScBrI is a stable intrinsic FV semiconductor with a high  $T_C$  and a spontaneous valley polarization of 90 meV in the valence band based on first-principles calculations and Monte Carlo (MC) simulations. For the magnetization direction along OOP, the strain engineering can drive the Janus monolayer ScBrI to experience the changes from FV to HVM, to valley-nonequilibrium quantum anomalous Hall effect (VQAHE), to HVM, to FV. However, the observable valley polarization and novel VQAHE states are not generated for the IP condition. In the appropriate strain section, the Janus monolayer ScBrI does indeed own intrinsic OOP magnetic anisotropy, spontaneous valley polarization, and VQAHE states. These results emphasize that the Janus monolayer ScBrI can be an excellent candidate for valleytronic, spintronic, and topological applications.

## II. Computational details

In our work, first-principles calculations are performed utilizing the Vienna *ab initio* simulation package (VASP)<sup>42,43</sup> based on density functional theory (DFT). The relevant electronic structure is calculated by the projector-augmented wave (PAW) method,<sup>44</sup> and the exchange–correlation potentials are handled by the generalized gradient approximation (GGA) with the Perdew–Burke–Ernzerhof (PBE) functional.<sup>45</sup> The Monkhorst–Pack (MP) was selected to be  $19 \times 19 \times 1$ . The kinetic energy cut-off for the plane wave basis is set to 500 eV with a force convergence criterion of  $10^{-2}$  eV Å<sup>-1</sup> and an energy convergence criterion of  $10^{-6}$  eV. The thickness of the vacuum layer is set to 25 Å to avoid the influence of adjacent layers in the periodic boundary. The 3d orbitals of Sc atoms are treated using the PBE+ $U$  method,<sup>46-48</sup> and the Hubbard  $U$

parameter of 3 eV is chosen.<sup>33</sup> The HSE06 hybrid functional<sup>49</sup> is utilized in the calculations of electronic band structures to examine the reliability of electronic properties obtained from the PBE+ $U$  method. The phonon spectrum is acquired by the PHONOPY code<sup>50,51</sup> using a  $5 \times 5 \times 1$  supercell based on the density functional perturbation theory. By means of the maximally localized Wannier functions, the anomalous Hall conductivity (AHC), Berry curvature, and edge state are obtained in the WANNIER90 package.<sup>52,53</sup>

## III. Results and discussion

Fig. 1(a) exhibits the crystal structures of the Janus monolayer ScBrI, which consists of the Br–Sc–I sandwich layer. Analogously to 2H-MoSSe,<sup>54,55</sup> each Sc atom is surrounded by three Br and three I atoms, constituting a triangular prism. The optimized lattice constant is 3.91 Å using the PBE+ $U$

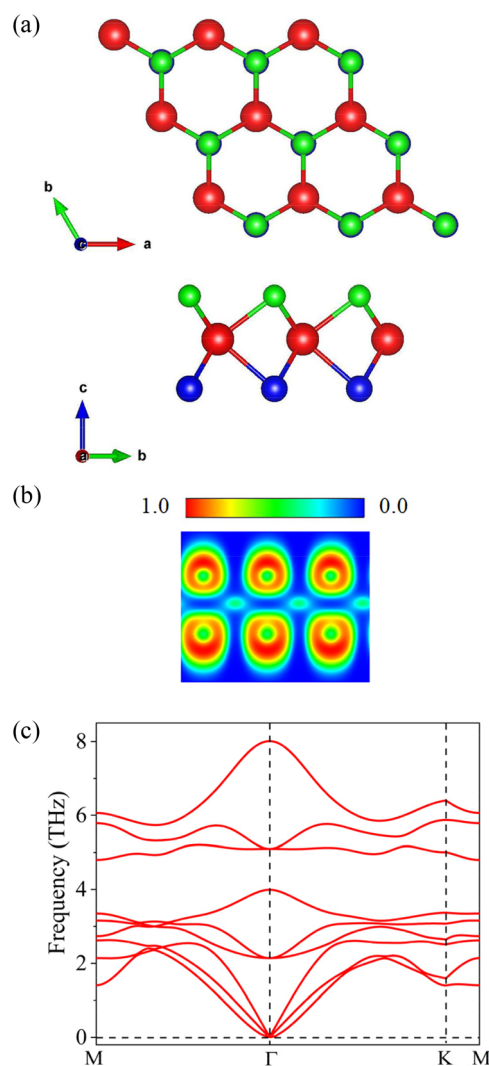


**Fig. 1** (a) Top and side views of the Janus monolayer ScBrI. The green, red, and blue atoms represent Br, Sc, and I, respectively. (c) ELF and (d) phonon dispersions of ScBrI.

method, and the space group is  $P3m1$  with broken inversion symmetry. The corresponding bond lengths of Sc–Br and Sc–I are 2.84 Å and 3.00 Å, respectively. The Janus monolayer ScBrI can be constructed by replacing one of two I (Br) layers with Br (I) atoms in the  $\text{ScI}_2$  ( $\text{ScBr}_2$ ) monolayers. We calculate the formation energy by  $E_{\text{form}} = (\mu_{\text{Sc}} + \mu_{\text{Br}} + \mu_{\text{I}} - E_{\text{ScBrI}})/3$ , where  $E_{\text{ScBrI}}$  is the total energy of the Janus monolayer ScBrI, and  $\mu_{\text{Sc}}$ ,  $\mu_{\text{Br}}$ , and  $\mu_{\text{I}}$  are the energy per Sc, Br, and I atoms in their corresponding most stable phases, respectively. It is found that  $E_{\text{form}}$  is about 0.81 eV per unit cell, implying the preference for the Janus monolayer ScBrI formation rather than the pure Sc, Br, and I phases. The electron localization function (ELF) was obtained to investigate the bonding characteristics of the Janus monolayer ScBrI, as shown in Fig. 1(b). Obviously, for the Sc–Br (Sc–I) bond, the electrons are highly localized around each of the Sc and Br(I) atoms, suggesting the typical ionic bonding between Sc and Br(I) atoms. No imaginary frequency is found in the calculated phonon spectra (see Fig. 1(c)), which demonstrates that the Janus monolayer ScBrI is dynamically stable.

The valence electronic configuration of Sc atom is  $3d^14s^2$ . After distributing two electrons to the surrounding Br and I atoms, just one valence electron is left, generating the magnetic moment of  $1\mu_{\text{B}}$  in per unit cell for the Janus monolayer ScBrI. In order to evaluate the magnetic ground state, the related magnetic configurations of the  $2 \times 2 \times 1$  supercell are shown in Fig. S1 of the ESI.† The FM configuration is discovered to be 240 meV per unit cell, smaller than the energy of the AFM configuration, which indicates that the Janus monolayer ScBrI always prefers FM coupling. The FM ground state of the Janus monolayer ScBrI is relevant to the crystal structure. As is illustrated in Fig. 1(a), the Sc–Br–Sc and Sc–I–Sc bonding angles are  $86.95^\circ$  and  $81.36^\circ$ , respectively, closing to  $90.0^\circ$ . The exchange interaction should be dominated by FM coupling on the basis of the Goodenough–Kanamori–Anderson rules. In view of the significant role of magnetic anisotropy for realizing the novel electronic states and long-range magnetic order in 2D materials, we obtain the magnetic anisotropy energy (MAE) from the difference in the acquired total energies with the magnetization direction perpendicular or parallel to the plane of the Janus monolayer ScBrI ( $E_{\text{MAE}} = E_{(100)} - E_{(001)}$ ). Therefore, the negative or positive MAE values mean that the easy magnetization axes are parallel or perpendicular to the plane of the monolayer, respectively. The MAE is calculated to be  $-0.22$  meV per unit cell, which indicates that the Janus monolayer ScBrI prefers IP magnetization in nature.

In the following, based on the classical 2D Heisenberg Hamiltonian model, the  $T_{\text{C}}$  of the Janus monolayer ScBrI is evaluated using MC simulations, which should be compared with the room temperature for practical applications of valleytronic and spintronic nanodevices. The spin Hamiltonian can be written as

$$H = \sum_{ij} J_1 S_i S_j - \sum_{ik} J_2 S_i S_k - AS_i^z S_y^z, \quad (1)$$

where  $J_1$ ,  $J_2$ ,  $A$ ,  $S_i$ , and  $S_i^z$  are the nearest neighbor (NN), next-nearest neighbor (NNN) magnetic exchange interaction parameters, anisotropy parameter, spin vector of each atom, and the component of the spin vector along  $Z$  direction, respectively. Fig. 2 exhibits the temperature-dependent magnetic moment in the unit cell. The magnetic moment starts to drop dramatically at 529 K, which implies the formation of paramagnetic (PM) state. To better comprehend the transition of FM to PM, the heat capacity ( $C_{\text{V}}$ ) is further acquired using the equation

$$C_{\text{V}} = \frac{\langle E^2 \rangle - \langle E \rangle^2}{L^2 T^2} \quad (2)$$

here,  $E$  is the total energy for each magnetic configuration. As shown in Fig. 2, the FM–PM phase transition appears at 529 K, which is drastically larger than those recently reported in the experimental field, such as bilayer  $\text{Cr}_2\text{Ge}_2\text{Te}_6$  (30 K)<sup>24</sup> and monolayer  $\text{CrI}_3$  (45 K).<sup>25</sup>

For the sake of acquiring accurate electronic properties, the influence of  $U$  value on electronic band structures is tested, which is exhibited in Fig. S2.† One can find that the Janus monolayer ScBrI is an indirect band-gap semiconductor between  $U = 0$  eV and 2.5 eV. When  $U$  value increases to 3 eV, the Janus monolayer ScBrI becomes a semiconductor with a direct band gap (see Fig. 3b), and the conduction band minimum (CBM) and valence band maximum (VBM) with the same spin are located in  $-K$  point, which is almost in agreement with the electronic band structure acquired from the HSE06 functional (see Fig. S3†). Hence, we select  $U = 3$  eV in the following discussion to investigate the electronic and topological properties. Fig. 3(a) exhibits the spin-polarized electronic band structure of the Janus monolayer ScBrI. When considering spin polarization but without SOC, the spin degeneracy is increased, generating a semiconducting feature with a direct band gap of 0.44 eV. Interestingly, the band edges at the  $+K$  and  $-K$  points present a pair of degenerate valleys in the valence and conduction bands. By further taking into account the SOC and IP magnetization orientation, the valley degeneracy is preserved, showing that the valley polarization is absent for the Janus monolayer ScBrI. This means the valley-polarized physical properties, such as anomalous valley Hall effect (AVHE) and quantum anomalous Hall (QAH) effect, do not

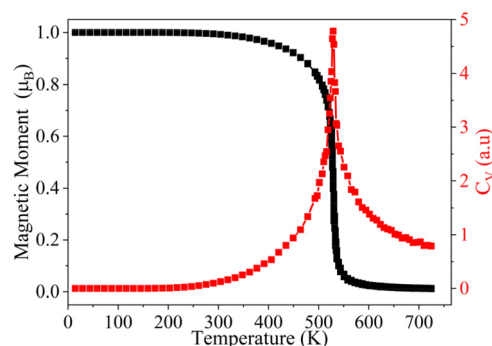
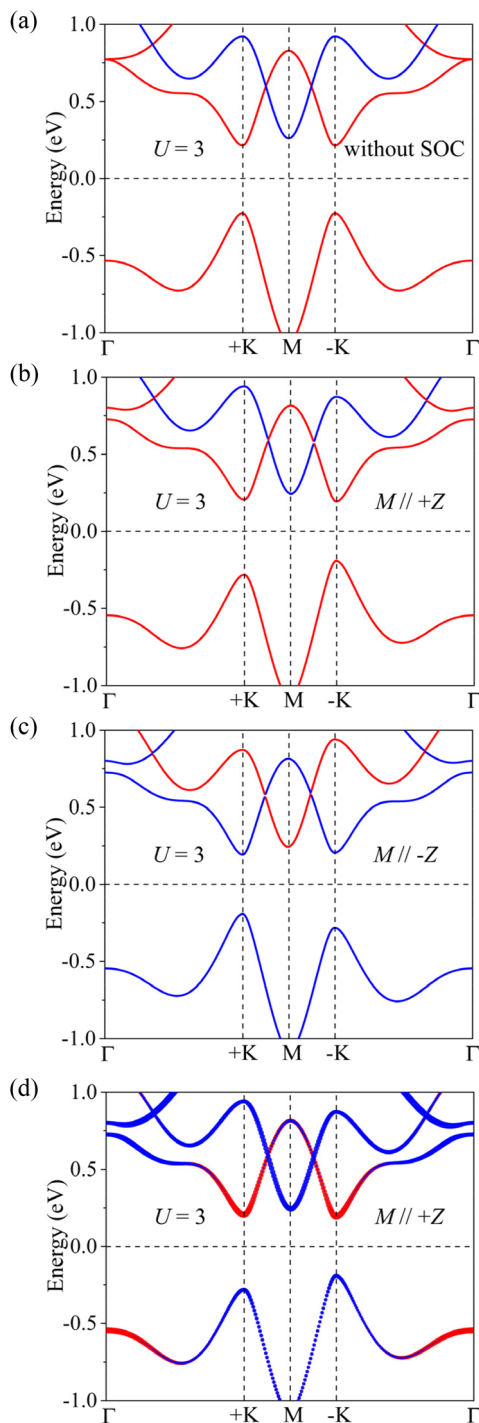


Fig. 2 Magnetic moment and  $C_{\text{V}}$  of ScBrI as a function of temperature.



**Fig. 3** Spin-polarized band structures of ScBrI (a) without and (b) with SOC effect. (c) The same as (b) but with the opposite magnetization direction. Red and blue lines express spin-up and spin-down states, respectively. (d) The orbital-resolved band structure of ScBrI with SOC when the magnetization direction is along +Z. Red and blue symbols represent the  $d_{z^2}$  and  $d_{x^2-y^2}/d_{xy}$  orbital components of Sc, respectively.

appear in the Janus monolayer ScBrI in nature. For the sake of exploring the valley-polarized physical properties, we assume that the magnetization orientation of the Janus monolayer

ScBrI is tuned from IP to OOP in the following discussion. As we will show later, strain engineering can adjust the magnetization orientation.

The band structure of the Janus monolayer ScBrI with SOC and OOP magnetization is exhibited in Fig. 3(b). It is worth noting that the SOC reduces the degeneracy between the +K and -K valley states (the energy of -K valley state is higher than +K valley's) in the valence band, resulting in a spontaneous valley polarization of 90 meV in the Janus monolayer ScBrI, which is equivalent to using a large external magnetic field of around 450–900 T. The valley polarization of the Janus monolayer ScBrI is larger than those of reported FV materials, such as VAgP<sub>2</sub>Se<sub>6</sub> (15 meV),<sup>56</sup> TiVI<sub>6</sub> (22 meV),<sup>57</sup> LaBr<sub>2</sub> (33 meV),<sup>58</sup> and Vsi2N4 (63 meV).<sup>28</sup> In order to be a useful valley material, it is critically essential to break the degeneracy between the +K and -K valleys, and the valley polarization should be large enough to conquer the thermal noise. Hence, such a fine valley polarization of the Janus monolayer ScBrI will lead to nonvolatile valley polarization and easy manipulation of valley states for logic applications at room temperature. In addition, there is a nontrivial band inside the energy window of -1 to 0 eV. The external magnetic field can tune the valley polarization of the Janus monolayer ScBrI. As shown in Fig. 3(c), the valley polarization can be flipped by reversing the magnetization of Sc atoms, that is, the -K valley has a lower energy than +K valley. When the Fermi level ( $E_F$ ) is moved to the energy section between -K and +K valleys, the carriers come from +K valley in the spin-up channel. This provides an efficient means to regulate the valley properties of the Janus monolayer ScBrI by manipulating the direction of magnetization. All in all, combined with the  $T_C$  discussed above, the Janus monolayer ScBrI is a desired FV semiconductor for practical applications, such as valley valves, nonvolatile magnetic random access memory, valley filters, and other spintronic and valleytronic devices.

The potential physics of spontaneous valley polarization in the Janus monolayer ScBrI is put down to the joint influences of the strong SOC and intrinsic magnetic exchange field. As exhibited in Fig. 3(a), with the spin polarization but excepting SOC, the spin-down and spin-up states are completely split on account of the magnetic exchange interaction, whereas the degeneracy of energy between +K and -K valleys is maintained. The orbital projected band structure is plotted to investigate the orbital contribution. According to Fig. 3(d), the -K and +K valleys in the conduction bands are mainly contributed by  $d_{z^2}$  orbitals, while those in the valence bands are mainly contributed by  $d_{xy}$  and  $d_{x^2-y^2}$  orbitals. Given that the SOC plays a key part in the spontaneous valley polarization of the Janus monolayer ScBrI, a simple theory is next built to further elucidate the nature of the valley polarization. The SOC Hamiltonian can be written as

$$\hat{H}_{\text{SOC}} = \lambda \hat{L} \cdot \hat{S} = \hat{H}_{\text{SOC}}^0 + \hat{H}_{\text{SOC}}^1, \quad (3)$$

where  $\lambda$  is the coupling constant. The states around the +K and -K valleys are composed of the same spin channel due to the

spin polarization. So the interaction disappears between opposite spin states,  $\hat{H}_{\text{SOC}}^1 = 0$ , and the interaction shows between the same spin states:

$$\hat{H}_{\text{SOC}} \approx \hat{H}_{\text{SOC}}^0 = \lambda \hat{S}_{Z'} \left( \hat{L}_Z \cos \theta + \frac{1}{2} \hat{L}_+ e^{-i\theta} \sin \theta + \frac{1}{2} \hat{L}_- e^{+i\theta} \sin \theta \right) \quad (4)$$

Here,  $\hat{L}_Z$  and  $\hat{S}_{Z'}$  are the  $Z/Z'$  component of the orbital and spin angular momentum operators, respectively. Both the  $\phi$  and  $\theta$  define the spin orientation, which refer to the polar angles, and  $\hat{L}_\pm = \hat{L}_x \pm i\hat{L}_y$ . On the basis of symmetry of the wave vector at the +K and -K valleys and the contribution of orbitals to the band edges, the basis functions are selected as follows:

$$|\phi_v^\tau\rangle = \sqrt{\frac{1}{2}} (|d_{x^2-y^2}\rangle + i\tau|d_{xy}\rangle) \quad (5)$$

and

$$|\phi_c^\tau\rangle = |d_{z^2}\rangle, \quad (6)$$

where v and c denote the valence and conduction bands, respectively, and  $\tau = \pm 1$  refers to the valley index at the  $\pm K$  valleys. Energy levels at the +K and -K valleys are defined as:

$$E_c^\tau = \langle \phi_c^\tau | \hat{H}_{\text{SOC}}^0 | \phi_c^\tau \rangle \quad (7)$$

$$E_v^\tau = \langle \phi_v^\tau | \hat{H}_{\text{SOC}}^0 | \phi_v^\tau \rangle \quad (8)$$

If the magnetic moment is along the OOP direction ( $\theta = 0$ ), eqn (4) can be simplified as:

$$\hat{H}_{\text{SOC}}^0 = \lambda \hat{S}_{Z'} \hat{L}_Z = \alpha \hat{L}_Z \quad (9)$$

Accordingly, the valley polarizations at the +K and -K valleys of the valence and conduction bands are given by

$$E_v^- - E_v^+ = i \langle d_{x^2-y^2} | \hat{H}_{\text{SOC}}^0 | d_{xy} \rangle - i \langle d_{xy} | \hat{H}_{\text{SOC}}^0 | d_{x^2-y^2} \rangle = 4\alpha \quad (10)$$

$$E_c^- - E_c^+ = 0 \quad (11)$$

Here we make use of  $\hat{L}_z |d_{x^2-y^2}\rangle = 2i |d_{xy}\rangle$  and  $\hat{L}_z |d_{xy}\rangle = -2i |d_{x^2-y^2}\rangle$ . As the first-order perturbation of the SOC effect, these discussions validate that the valley degeneracy is removed at the +K and -K valleys of the valence bands, but it still persisted in the conduction band, consistent with the first-principles calculations.

Due to a break in the intrinsic inversion symmetry in the Janus monolayer ScBrI, the charge carriers at the +K and -K valleys will gain a valley-contrasting Berry curvature. By derivation from the Kubo formula,<sup>59</sup> the Berry curvature can be written as the summation of all occupied states:

$$\Omega(k) = - \sum_n \sum_{n \neq n'} f_n(k) \frac{2 \text{Im} \langle \psi_{nk} | \hat{v}_x | \psi_{n'k} \rangle \langle \psi_{n'k} | \hat{v}_y | \psi_{nk} \rangle}{(E_n - E_{n'})^2}, \quad (12)$$

where  $f_n(k)$  is the Fermi-Dirac distribution function,  $k$  is the electron wave vector,  $\hat{v}_x$  is the  $x$  component of the velocity oper-

ator, and  $E_n$  is the eigenvalue of the Bloch wave function  $\psi_{nk}$ . Fig. 4(a) and (b) depict the obtained Berry curvature of the Janus monolayer ScBrI in the 2D BZ and along the high-symmetry points, respectively. We can observe that the Berry curvature is significantly peaked at the +K and -K valleys, and it decays quickly to zero. Because of the absence of inversion symmetry, it is expected that the Berry curvature exhibits the opposite signs at two valleys, which demonstrates the robust valley-contrasting trait in the Janus monolayer ScBrI. For this case, the nonzero Berry curvature along OOP can serve as a magnetic field in the existence of an IP longitudinal electric field  $E$ , supplying an anomalous transversal velocity to the charge carriers:

$$\nu_\perp = -\frac{e}{\hbar} E \times \Omega(k) \quad (13)$$

In this way, the Bloch electrons in different valleys can move to the opposite transversal edges of the Janus monolayer ScBrI, giving rise to the valley Hall effect. Moreover, the spin Hall effect can also be realized when taking into consideration the spin-valley coupling. More significantly, it can be found from Fig. 4(a) and (b) that the Berry curvature has different magnitudes at the +K and -K valleys due to a break in the time reversal symmetry. When the magnetization of Sc atoms is reversed, the absolute values at two valleys will be exchanged, while their signs remain unchanged. An appropriate hole doping that adjusts the Fermi level between the +K

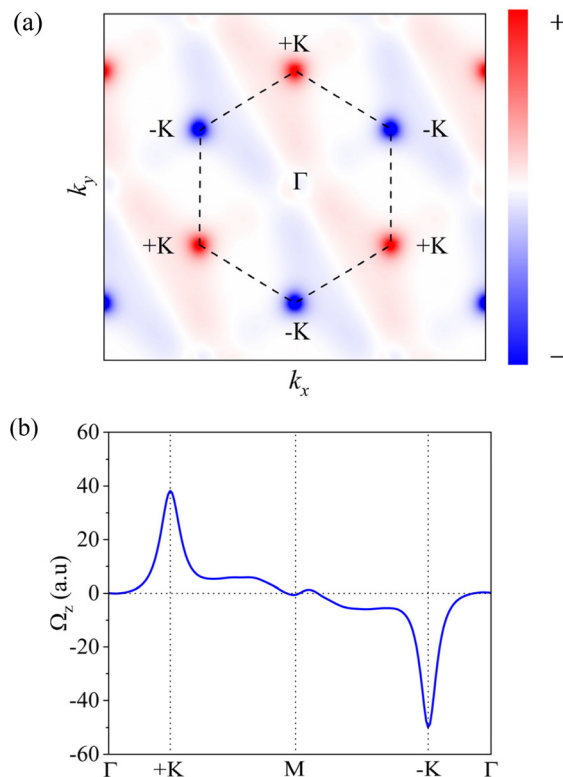
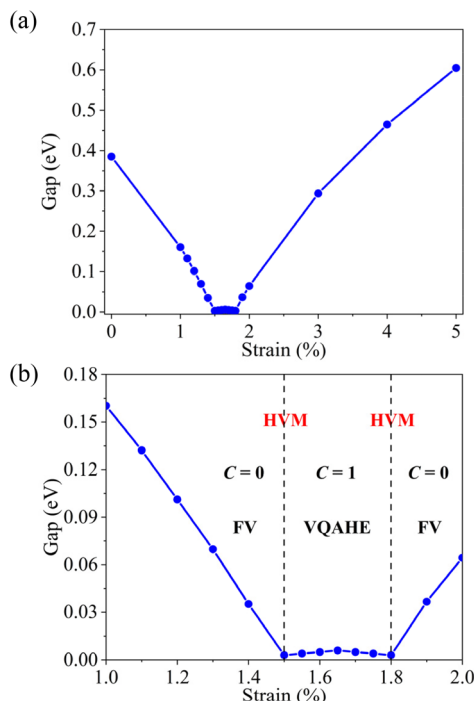


Fig. 4 Berry curvature of ScBrI (a) in the 2D BZ and (b) along the high-symmetry points.

and  $-K$  valleys of the valence band can make the doped holes collect on one boundary of the Janus monolayer ScBrI under an IP longitudinal electric field, generating net Hall currents along the transverse direction. So, AVHE can be realized in the Janus monolayer ScBrI. For the direction of magnetization from the positive to negative, it is worth noting that the net Hall current is opposite, which can be measured easily in the experiment. Because the accumulated net hole charges are contributed by the same valley with identical spin orientation, the spin, transversal charge, and valley Hall currents occur simultaneously, which facilitate the practical valleytronic applications and the detection of valley pseudospin. Except for hole doping, the AVHE can be achieved as well for the 2D hexagonal system by means of the valley-dependent optical selection rule,<sup>60</sup> where the photoexcited electrons and holes will transfer to the opposite transversal sides of the Janus monolayer ScBrI under an IP longitudinal electric field, indicating that the total energy of incident light locates between the band gap values in the  $+K$  and  $-K$  valleys.

Considering that any 2D systems will inevitably undergo structural modifications in the synthesis process when growing on the substrates, it is mandatory to investigate the influence of strain on the electronic, magnetic, and topological properties of the Janus monolayer ScBrI for its practical applications in valleytronic and spintronic nanodevices. In this work, biaxial strain in a rational range of  $\pm 5\%$  is applied, which is defined as  $\epsilon = (a - a_0)/a_0$ , with  $a$  and  $a_0$  being the lattice constants of the Janus monolayer ScBrI in the strained and unstrained states, respectively. The negative and positive  $\epsilon$  values express, respectively, the compressive and tensile strains. For the sake of examining the magnetic ground state of the strained Janus monolayer ScBrI, the energy differences  $\Delta E$  between AFM and FM states are calculated employing a  $2 \times 2 \times 1$  supercell, which is shown in Fig. S4.† We find that the Janus monolayer ScBrI prefers the FM ground state for all strained states, and the FM interaction increases monotonically with the strain value from  $-5\%$  to  $5\%$ , thus yielding the rising  $T_C$ . The variation of MAE under different strains is shown in Fig. S5.† The MAE of the Janus monolayer ScBrI is along the OOP at  $1\% \leq \epsilon \leq 1.8\%$ ; however, when  $-5\% \leq \epsilon < 1\%$  and  $1.8\% < \epsilon \leq 5\%$ , the system prefers IP magnetization.

Next, the electronic structures of the Janus monolayer ScBrI under different strains are acquired by GGA + SOC +  $U$ . For compressive strain, the CBM and VBM are located in M and  $-K$  points, respectively, showing a feature of indirect gap semiconductor (see Fig. S6†), so the tensile strain is analysed primarily in the following discussion. For various MVC phases in the Janus monolayer ScBrI, Fig. 5 and 6 exhibit the total electronic band gaps and the representative band structures under different biaxial strains, respectively. As is illustrated in Fig. 5(a) and (b), when  $0 < \epsilon < 1.5\%$ , with increasing tensile strain, the band gap decreases. However, the band gap increases with increasing tensile strain for  $1.8\% < \epsilon < 5\%$ . We can find very little band gap between  $\epsilon = 1.5\%$  and  $1.8\%$ , which may reveal the novel nontrivial topological properties. For  $0 < \epsilon < 1.5\%$ , there is a fine valley polarization at the  $+K$



**Fig. 5** (a) Band gaps of ScBrI as a function of biaxial strain (0–5%). (b) Enlarged view of the 1%–2% portion, along with a phase diagram under different biaxial strains.

and  $-K$  points in the valence bands, and the  $-K$  valley is polarized. But the noteworthy valley polarization happens in the conduction bands for  $1.8\% < \epsilon < 5\%$ , and the  $+K$  valley is polarized. In the two sections, the Janus monolayer ScBrI is a FV material. Around  $\epsilon = 1.5\%$ , the system is gapless in the  $-K$  point, while it is gapped in the  $+K$  point, building a half-valley-metal (HVM) state (see Fig. 6(b)). Analogous to the half-metal materials in spintronics with intrinsic 100% spin polarization, the HVM state can accomplish 100% valley polarization in valleytronics.<sup>35</sup> Since the SOC effect is incorporated in calculations, the HVM state of the same spin channel indicates 100% absolute spin polarization, in contrast to the traditional half-metal materials, where the SOC effect usually mixes the spin-down and spin-up bands.<sup>61,62</sup> The HVM state can also be discovered at around  $\epsilon = 1.8\%$  (see Fig. 6(d)), but the band gap disappears at the  $+K$  point, and then is reopened for the  $-K$  point. As the gap closes, reopens, and closes, this indicates there may be a topological phase transition between the two HVM states.

The electronic band structures of the Sc-d-orbital properties for  $\epsilon = 1\%$ ,  $\epsilon = 1.65\%$ , and  $\epsilon = 2\%$  are exhibited in Fig. S7.† For all strained states, the  $+K$  and  $-K$  valleys of the conduction and valence bands are primarily determined by  $d_{z^2}$  and  $d_{x^2-y^2}/d_{xy}$  orbitals. The  $+K$  and  $-K$  valleys of the conduction bands are determined by  $d_{z^2}$  orbitals for  $0 < \epsilon < 1.5\%$ , while those in the valence bands are determined by  $d_{x^2-y^2}$  and  $d_{xy}$  orbitals (see Fig. S7(a)†). For  $1.8\% < \epsilon < 5\%$ , the opposite situation can be found (see Fig. S7(c)†). When  $1.5\% < \epsilon < 1.8\%$ , the  $+K$  valley

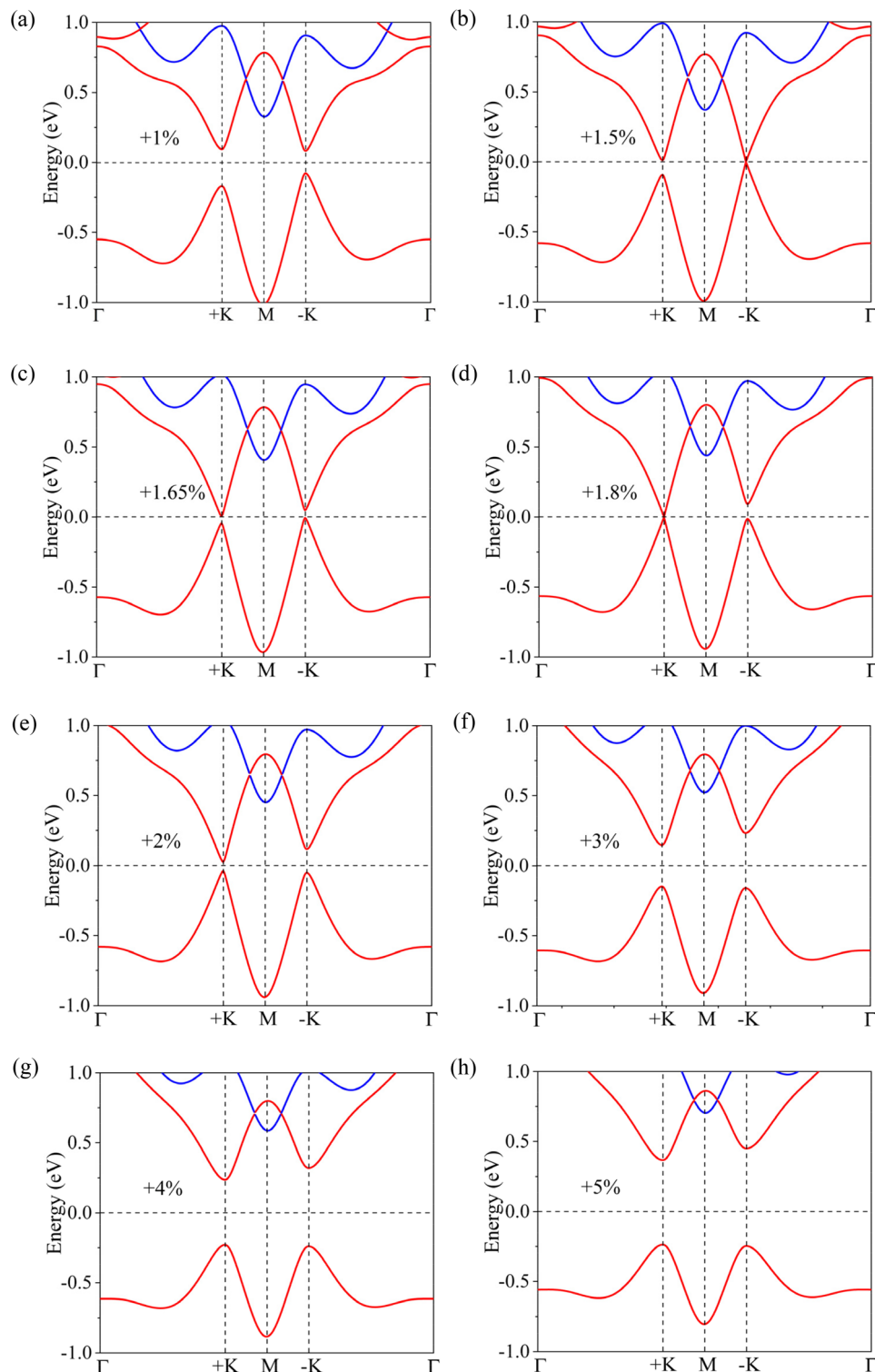


**Fig. 6** Energy band structures of ScBrI under different biaxial strains. The red and blue lines express spin-up and spin-down states, respectively.

in the conduction band and the  $-K$  valley in the valence bands are determined by  $d_{z^2}$  orbitals, and the  $+K$  valley in the valence bands and the  $-K$  valley in the conduction band are determined by  $d_{x^2-y^2}$  and  $d_{xy}$  orbitals (see Fig. S7(b)†). It seems to imply that the topological phase transitions are strongly

associated with the band inversion of  $d_{x^2-y^2}/d_{xy}$  and  $d_{z^2}$  orbitals. As is shown in Fig. S8,† the Berry curvatures of representative strained states ( $\epsilon = 1\%$ ,  $\epsilon = 1.65\%$ , and  $\epsilon = 2\%$ ) are acquired. It is notable that the Berry curvature of the Janus monolayer ScBrI is peaked for the  $+K$  and  $-K$  valleys in all

strained states. The Berry curvatures have opposite signs and different absolute values at the +K and -K valleys for  $0 < \epsilon < 1.5\%$  and  $1.8\% < \epsilon < 5\%$  (see Fig. S8(a), (c), (d), and (f)†). When  $\epsilon = 1\%$  and  $2\%$ , since the contribution of the integration of Berry curvatures at the +K and -K valleys are opposite, the Chern number is usually zero. Nevertheless, for  $1.5\% < \epsilon < 1.8\%$ , the Berry curvatures possess different magnitudes and the same signs (see Fig. S8(b) and (e)†). The Berry curvatures of the +K and -K valleys have the same sign for  $\epsilon = 1.65\%$ , illustrating that a nonzero Chern number can be obtained by integrating the Berry curvature of the first BZ.

The chiral edge state and AHC of  $\epsilon = 1.65\%$  are calculated to prove the QAH phases, which are plotted in Fig. 7. The AHC is obtained by integrating the Berry curvature in the first BZ:<sup>63,64</sup>

$$\sigma_{xy} = -\frac{e^2}{\hbar} \int \frac{dk}{(2\pi)^2} \Omega(k) \quad (14)$$

here,  $e$ ,  $\hbar$ , and  $\Omega(k)$  are the electronic charge, reduced Planck constant, and Berry curvature. We acquire a quantized AHC  $e^2/h$  (see Fig. 7(a)) by integrating the Berry curvature, which indicates nontrivial topological property with  $C = 1$ . As shown in Fig. 7(b), we further observe a gapless chiral edge state linking the valence and conduction bands, consistent with the calculations of the Chern number. All of these indicators prove that the Janus monolayer ScBrI at 1.65% strain possesses the QAH phase. It is distinctly found that the QAH phase can coexist with the valley properties of the conduction and valence bands, and the -K and +K valleys are intrinsically polarized. It

is referred to as VQAHE due to the combination of nontrivial band topology with valleytronics and spintronics, providing a fantastic platform to investigate the interplay between topology physics and valley properties. Strikingly, under the precondition of OOP magnetization, the Janus monolayer ScBrI can be transitioned into a VQAHE phase under tensile strains between 1.5% and 1.8%, which is featured with a unit Chern number and a single chiral edge state. It is notable that the strain range from 1.5% to 1.8% is easy to realize in the experiment. For  $-5\% < \epsilon < 1\%$  and  $1.8\% < \epsilon < 5\%$ , although the easy magnetic axis direction of the Janus monolayer ScBrI is along the IP, it can be adjusted into OOP by a small external magnetic field on account of the small MAE. However, it must be stressed that VQAHE with the valley index has apparent discrepancy compared with the valley-polarized quantum anomalous Hall effect (VPQAHE).<sup>65,66</sup> Firstly, VQAHE is caused by nonequilibrium Berry curvature in the +K and -K valleys, and combines the QAH effect and valley index. It is characterized by the non-integer valley Chern numbers and an integer Chern number. However, for VPQAHE, both the valley Chern number and Chern number are integers. Secondly, the nonzero Chern number of the VQAHE originates from two different valleys, while the chiral edge state of the VPQAHE is connected by the same valley (that is to say, the nonzero Chern number originates from only one valley).

## IV. Conclusion

In short, we have conducted a systematic research on the versatile Janus monolayer ScBrI by means of the combination of MC simulations, first-principles calculations, and strain engineering. Based on the stable structure, the 2D system is forecasted to be an intrinsic FV semiconductor that not only expresses high  $T_C$  but also realizes an appreciable spontaneous valley polarization in the valence band. Strikingly, under intrinsic OOP magnetization, the Janus monolayer ScBrI can be turned to a VQAHE phase between the 1.5% and 1.8% tensile strains, which is characterized by a unit Chern number and a single chiral edge state. The topological phase transitions are closely connected with a band inversion between  $d_{x^2-y^2}/d_{xy}$  and  $d_{z^2}$  orbitals, and a sign-reversible Berry curvature at the +K and -K valleys. The boundaries of the VQAHE phase can be regarded as two significant HVM states. These fascinating characteristics would potentially offer the 2D material a wide range of practical applications in topological, valleytronic, and spintronic electronics and their integration. It is hoped that this research will encourage the future exploration and fabrication of the Janus monolayer ScBrI.

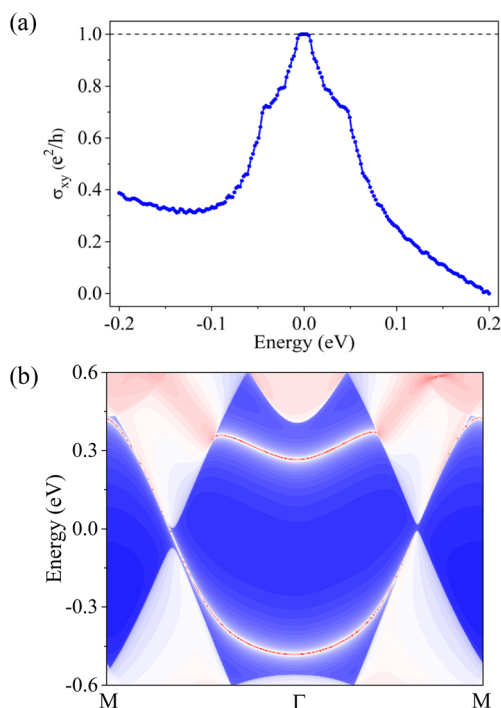


Fig. 7 (a) AHC and (b) topological edge state of ScBrI with  $\epsilon = 1.65\%$ .

## Conflicts of interest

There are no conflicts of interest to declare.



## Acknowledgements

This work was supported by National Natural Science Foundation of China (Grant No. 52173283), Taishan Scholar Program of Shandong Province (Grant No. ts20190939), Independent Cultivation Program of Innovation Team of Jinan City (Grant No. 2021GXRC043), National Natural Science Foundation of China (Grant No. 12004137), and Natural Science Foundation of Shandong Province (Grant No. ZR2020QA052).

## References

- X. Tang and L. Kou, Two-dimensional ferroics and multi-ferroics: platforms for new physics and applications, *J. Phys. Chem. Lett.*, 2019, **10**, 6634–6649.
- J. Chu, Y. Wang, X. Wang, K. Hu, G. Rao, C. Gong, C. Wu, H. Hong, X. Wang, K. Liu, C. Gao and J. Xiong, 2D Polarized Materials: Ferromagnetic, Ferrovalley, Ferroelectric Materials, and Related Heterostructures, *Adv. Mater.*, 2021, **33**, 2004469.
- Z. Liu, L. Deng and B. Peng, Ferromagnetic and ferroelectric two-dimensional materials for memory application, *Nano Res.*, 2021, **14**, 1802–1813.
- A. Rycerz, J. Tworzydło and C. W. J. Beenakker, Valley filter and valley valve in graphene, *Nat. Phys.*, 2007, **3**, 172–175.
- D. Xiao, W. Yao and Q. Niu, Valley-contrasting physics in graphene: magnetic moment and topological transport, *Phys. Rev. Lett.*, 2007, **99**, 236809.
- J. R. Schaibley, H. Yu, G. Clark, P. Rivera, J. S. Ross, K. L. Seyler, W. Yao and X. Xu, Valleytronics in 2D materials, *Nat. Rev. Mater.*, 2016, **1**, 16055.
- W. R. Liu, X. J. Dong, Y. Z. Lv, W. X. Ji, Q. Cao, P. J. Wang, F. Li and C. W. Zhang, Magnetic anisotropy and ferroelectric-driven magnetic phase transition in monolayer Cr<sub>2</sub>Ge<sub>2</sub>Te<sub>6</sub>, *Nanoscale*, 2022, **14**, 3632–3643.
- L. Zhang, S. F. Zhang, W. X. Ji, C. W. Zhang, P. Li, P. J. Wang, S. S. Li and S. S. Yan, Discovery of a novel spin-polarized nodal ring in a two-dimensional HK lattice, *Nanoscale*, 2018, **10**, 20748–20753.
- S. J. Zhang, C. W. Zhang, S. F. Zhang, W. X. Ji, P. Li, P. J. Wang, S. S. Li and S. S. Yan, Intrinsic Dirac half-metal and quantum anomalous Hall phase in a hexagonal metal-oxide lattice, *Phys. Rev. B*, 2017, **96**, 205433.
- S. S. Li, W. X. Ji, S. J. Hu, C. W. Zhang and S. S. Yan, Effect of Amidogen Functionalization on Quantum Spin Hall Effect in Bi/Sb(111) Films, *ACS Appl. Mater. Interfaces*, 2017, **9**, 41443–41453.
- Y. P. Wang, W. X. Ji, C. W. Zhang, P. Li, S. F. Zhang, P. J. Wang, S. S. Li and S. S. Yan, Two-dimensional arsenene oxide: A realistic large-gap quantum spin Hall insulator, *Appl. Phys. Lett.*, 2017, **110**, 213101.
- M. H. Zhang, C. W. Zhang, P. J. Wang and S. S. Li, Prediction of high-temperature Chern insulator with half-metallic edge states in asymmetry-functionalized stanene, *Nanoscale*, 2018, **10**, 20226–20233.
- X. J. Dong, M. J. Ren and C. W. Zhang, Quantum anomalous Hall effect in germanene by proximity coupling to a semiconducting ferromagnetic substrate NiI<sub>2</sub>, *Phys. Chem. Chem. Phys.*, 2022, **24**, 21631–21637.
- D. Xiao, G. B. Liu, W. Feng, X. Xu and W. Yao, Coupled Spin and Valley Physics in Monolayers of MoS<sub>2</sub> and Other Group-VI Dichalcogenides, *Phys. Rev. Lett.*, 2012, **108**, 196802.
- S. A. Vitale, D. Nezich, J. O. Varghese, P. Kim, N. Gedik, P. Jarillo-Herrero, D. Xiao and M. Rothschild, Valleytronics: opportunities, challenges, and paths forward, *Small*, 2018, **14**, 1801483.
- Y. Liu, Y. Gao, S. Zhang, J. He, J. Yu and Z. Liu, Valleytronics in transition metal dichalcogenides materials, *Nano Res.*, 2019, **12**, 2695–2711.
- S. Zhao, X. Li, B. Dong, H. Wang, H. Wang, Y. Zhang, Z. Han and H. Zhang, Valley manipulation in monolayer transition metal dichalcogenides and their hybrid systems: status and challenges, *Rep. Prog. Phys.*, 2021, **84**, 026401.
- D. MacNeill, C. Heikes, K. F. Mak, Z. Anderson, A. Kormanyos, V. Zolyomi, J. Park and D. C. Ralph, Breaking of Valley Degeneracy by Magnetic Field in Monolayer MoSe<sub>2</sub>, *Phys. Rev. Lett.*, 2015, **114**, 037401.
- P. Back, M. Sidler, O. Cotlet, A. Srivastava, N. Takemura, M. Kroner and A. Imamoglu, Giant Paramagnetism-Induced Valley Polarization of Electrons in Charge-Tunable Monolayer MoSe<sub>2</sub>, *Phys. Rev. Lett.*, 2017, **118**, 237404.
- R. Peng, Y. Ma, S. Zhang, B. Huang and Y. Dai, Valley Polarization in Janus Single-Layer MoSSe via Magnetic Doping, *J. Phys. Chem. Lett.*, 2018, **9**, 3612–3617.
- J. Li, L. Gu and R. Wu, Possible realization and protection of valley-polarized quantum Hall effect in Mn/WS<sub>2</sub>, *Phys. Rev. B*, 2020, **101**, 024412.
- C. Zhao, T. Norden, P. Zhang, P. Zhao, Y. Cheng, F. Sun, J. P. Parry, P. Taheri, J. Wang, Y. Yang, T. Scrace, K. Kang, S. Yang, G. Miao, R. Sabirianov, G. Kioseoglou, W. Huang, A. Petrou and H. Zeng, Enhanced valley splitting in monolayer WSe<sub>2</sub> due to magnetic exchange field, *Nat. Nanotechnol.*, 2017, **17**, 757–762.
- T. Norden, C. Zhao, P. Zhang, R. Sabirianov, A. Petrou and H. Zeng, Giant valley splitting in monolayer WS<sub>2</sub> by magnetic proximity effect, *Nat. Commun.*, 2019, **10**, 4163.
- C. Gong, L. Li, Z. Li, H. Ji, A. Stern, Y. Xia, T. Cao, W. Bao, C. Wang and Y. Wang, Discovery of intrinsic ferromagnetism in two-dimensional van der Waals crystals, *Nature*, 2017, **546**, 265–269.
- B. Huang, G. Clark, E. Navarro-Moratalla, D. R. Klein, R. Cheng, K. L. Seyler, D. Zhong, E. Schmidgall, M. A. McGuire and D. H. Cobden, Layer-dependent ferromagnetism in a van der Waals crystal down to the monolayer limit, *Nature*, 2017, **546**, 270–273.
- X. Wang, D. Li, Z. Li, C. Wu, C. M. Che, G. Chen and X. Cui, Ferromagnetism in 2D vanadium diselenide, *ACS Nano*, 2021, **15**, 16236–16241.
- W. Y. Tong, S. J. Gong, X. Wan and C. G. Duan, Concepts of ferrovalley material and anomalous valley Hall effect, *Nat. Commun.*, 2016, **7**, 13612.

- 28 Q. Cui, Y. Zhu, J. Liang, P. Cui and H. Yang, Spin-valley coupling in a two-dimensional  $\text{VSi}_2\text{N}_4$  monolayer, *Phys. Rev. B*, 2021, **103**, 085421.
- 29 K. Sheng, Q. Chen, H. K. Yuan and Z. Y. Wang, Monolayer  $\text{CeI}_2$ : An intrinsic room-temperature ferrovalley semiconductor, *Phys. Rev. B*, 2022, **105**, 075304.
- 30 P. Jiang, L. Kang, Y. L. Li, X. Zheng, Z. Zeng and S. Sanvito, Prediction of the two-dimensional Janus ferrovalley material  $\text{LaBrI}$ , *Phys. Rev. B*, 2021, **104**, 035430.
- 31 R. Li, J. Jiang, W. Mi and H. Bai, Room temperature spontaneous valley polarization in two-dimensional  $\text{FeClBr}$  monolayer, *Nanoscale*, 2021, **13**, 14807–14813.
- 32 T. Zhou, J. Zhang, H. Jiang, I. Zutic and Z. Yang, Giant spin-valley polarization and multiple Hall effect in functionalized bismuth monolayers, *npj Quantum Mater.*, 2018, **3**, 39.
- 33 Z. He, R. Peng, Y. Dai, B. Huang and Y. Ma, Single-layer  $\text{ScI}_2$ : A paradigm for valley-related multiple Hall effect, *Appl. Phys. Lett.*, 2021, **119**, 243102.
- 34 X. Kong, L. Li, L. Liang, F. M. Peeters and X. J. Liu, The magnetic, electronic, and light-induced topological properties in two-dimensional hexagonal  $\text{FeX}_2$  ( $X = \text{Cl}, \text{Br}, \text{I}$ ) monolayers, *Appl. Phys. Lett.*, 2020, **116**, 192404.
- 35 H. Hu, W. Y. Tong, Y. H. Shen, X. Wan and C. G. Duan, Concepts of the half-valley-metal and quantum anomalous valley Hall effect, *npj Comput. Mater.*, 2020, **6**, 129.
- 36 S. D. Guo, J. X. Zhu, M. Y. Yin and B. G. Liu, Substantial electronic correlation effects on the electronic properties in a Janus  $\text{FeClF}$  monolayer, *Phys. Rev. B*, 2022, **105**, 104416.
- 37 X. Zhou, R. W. Zhang, Z. Zhang, W. Feng, Y. Mokrousov and Y. Yao, Sign-reversible valley-dependent Berry phase effects in 2D valley-half-semiconductors, *npj Comput. Mater.*, 2021, **7**, 160.
- 38 S. Li, Q. Wang, C. Zhang, P. Guo and S. A. Yang, Correlation-driven topological and valley states in monolayer  $\text{VSi}_2\text{P}_4$ , *Phys. Rev. B*, 2021, **104**, 085149.
- 39 X. Feng, X. Xu, Z. He, R. Peng, Y. Dai, B. Huang and Y. Ma, Valley-related multiple Hall effect in monolayer  $\text{VSi}_2\text{P}_4$ , *Phys. Rev. B*, 2021, **104**, 075421.
- 40 H. Sun, S. S. Li, W. X. Ji and C. W. Zhang, Valley-dependent topological phase transition and quantum anomalous valley Hall effect in single-layer  $\text{RuClBr}$ , *Phys. Rev. B*, 2022, **105**, 195112.
- 41 S. D. Guo, W. Q. Mu and B. G. Liu, Valley-polarized quantum anomalous Hall insulator in monolayer  $\text{RuBr}_2$ , *2D Mater.*, 2022, **9**, 035011.
- 42 G. Kresse and J. Hafner, Ab initio molecular-dynamics simulation of the liquid-metal-amorphous-semiconductor transition in germanium, *Phys. Rev. B: Condens. Matter Mater. Phys.*, 1994, **49**, 14251.
- 43 G. Kresse and J. Furthmüller, Efficient iterative schemes for ab initio total-energy calculations using a plane-wave basis set, *Phys. Rev. B: Condens. Matter Mater. Phys.*, 1996, **54**, 11169.
- 44 P. E. Blochl, Projector augmented-wave method, *Phys. Rev. B: Condens. Matter Mater. Phys.*, 1994, **50**, 17953.
- 45 J. P. Perdew, K. Burke and M. Ernzerhof, Generalized Gradient Approximation Made Simple, *Phys. Rev. Lett.*, 1996, **77**, 3865.
- 46 S. L. Dudarev, G. A. Botton, S. Y. Savrasov, C. J. Humphreys and A. P. Sutton, Electron-energy-loss spectra and the structural stability of nickel oxide: An LSDA+U study, *Phys. Rev. B: Condens. Matter Mater. Phys.*, 1998, **57**, 1505.
- 47 V. I. Anisimov, J. Zaanen and O. K. Andersen, Band theory and Mott insulators: Hubbard U instead of Stoner I, *Phys. Rev. B: Condens. Matter Mater. Phys.*, 1991, **44**, 943.
- 48 Y. Zhang, L. F. Lin, A. Moreo and E. Dagotto, Theoretical study of the crystal and electronic properties of  $\alpha\text{-RuI}_3$ , *Phys. Rev. B*, 2022, **105**, 085107.
- 49 A. V. Krukau, O. A. Vydrov, A. F. Izmaylov and G. E. Scuseria, Influence of the exchange screening parameter on the performance of screened hybrid functionals, *J. Chem. Phys.*, 2006, **125**, 224106.
- 50 X. Wu, D. Vanderbilt and D. R. Hamann, Systematic treatment of displacements, strains, and electric fields in density-functional perturbation theory, *Phys. Rev. B: Condens. Matter Mater. Phys.*, 2005, **72**, 035105.
- 51 A. Togo, F. Oba and I. Tanaka, First-principles calculations of the ferroelastic transition between rutile-type and  $\text{CaCl}_2$ -type  $\text{SiO}_2$  at high pressures, *Phys. Rev. B: Condens. Matter Mater. Phys.*, 2008, **78**, 134106.
- 52 A. A. Mostofi, J. R. Yates, Y. S. Lee, I. Souza, D. Vanderbilt and N. Marzari, wannier90: A tool for obtaining maximally-localised Wannier functions, *Comput. Phys. Commun.*, 2008, **178**, 685–699.
- 53 X. Wang, J. R. Yates, I. Souza and D. Vanderbilt, Ab initio calculation of the anomalous Hall conductivity by Wannier interpolation, *Phys. Rev. B: Condens. Matter Mater. Phys.*, 2006, **74**, 195118.
- 54 A. Y. Lu, H. Zhu, J. Xiao, C. P. Chuu, Y. Han, M. H. Chiu, C. C. Cheng, C. W. Yang, K. H. Wei, Y. Yang, Y. Wang, D. Sokaras, D. Nordlund, P. Yang, D. A. Muller, M. Y. Chou, X. Zhang and L. J. Li, Janus monolayers of transition metal dichalcogenides, *Nat. Nanotechnol.*, 2017, **12**, 744–749.
- 55 J. Zhang, S. Jia, I. Kholmanov, L. Dong, D. Er, W. Chen, H. Guo, Z. Jin, V. B. Shenoy, L. Shi and J. Lou, Janus Monolayer Transition-Metal Dichalcogenides, *ACS Nano*, 2017, **11**, 8192–8198.
- 56 Z. Song, X. Sun, J. Zheng, F. Pan, Y. Hou, M.-H. Yung, J. Yang and J. Lu, Spontaneous valley splitting and valley pseudospin field effect transistors of monolayer  $\text{VAgP}_2\text{Se}_6$ , *Nanoscale*, 2018, **10**, 13986–13993.
- 57 W. Du, Y. Ma, R. Peng, H. Wang, B. Huang and Y. Dai, Prediction of single-layer  $\text{TiVI}_6$  as a promising two-dimensional valleytronic semiconductor with spontaneous valley polarization, *J. Mater. Chem. C*, 2020, **8**, 13220–13225.
- 58 P. Zhao, Y. Ma, C. Lei, H. Wang, B. Huang and Y. Dai, Single-layer  $\text{LaBr}_2$ : Two-dimensional valleytronic semiconductor with spontaneous spin and valley polarizations, *Appl. Phys. Lett.*, 2019, **115**, 261605.
- 59 D. J. Thouless, M. Kohmoto, M. P. Nightingale and M. den Nijs, Quantized Hall Conductance in a Two-

- Dimensional Periodic Potential, *Phys. Rev. Lett.*, 1982, **49**, 405.
- 60 G. Wang, C. Robert, M. M. Glazov, F. Cadiz, E. Courtade, T. Amand, D. Lagarde, T. Taniguchi, K. Watanabe, B. Urbaszek and X. Marie, In-plane propagation of light in transition metal dichalcogenide monolayers: optical selection rules, *Phys. Rev. Lett.*, 2017, **119**, 047401.
- 61 X. Li, X. Wu and J. Yang, Half-Metallicity in MnPSe<sub>3</sub> Exfoliated Nanosheet with Carrier Doping, *J. Am. Chem. Soc.*, 2014, **136**, 11065–11069.
- 62 K. Sheng, Z. Y. Wang, H. K. Yuan and H. Chen, Two-dimensional hexagonal manganese carbide monolayer with intrinsic ferromagnetism and half-metallicity, *New J. Phys.*, 2020, **22**, 103049.
- 63 T. Jungwirth, Q. Niu and A. H. MacDonald, Anomalous Hall Effect in Ferromagnetic Semiconductors, *Phys. Rev. Lett.*, 2002, **88**, 207208.
- 64 Y. Yao, L. Kleinman, A. H. MacDonald, J. Sinova, T. Jungwirth, D. S. Wang, E. Wang and Q. Niu, First Principles Calculation of Anomalous Hall Conductivity in Ferromagnetic bcc Fe, *Phys. Rev. Lett.*, 2004, **92**, 037204.
- 65 H. Pan, Z. Li, C.-C. Liu, G. Zhu, Z. Qiao and Y. Yao, Valley-polarized quantum anomalous Hall effect in silicene, *Phys. Rev. Lett.*, 2014, **112**, 106802.
- 66 J. Zhou, Q. Sun and P. Jena, Valley-polarized quantum anomalous Hall effect in ferrimagnetic honeycomb lattices, *Phys. Rev. Lett.*, 2017, **119**, 046403.